PNAS RESEARCH ARTICLE | MICROBIOLOGY

Structural and inhibitor sensitivity analysis of influenza B–like viral neuraminidases derived from Asiatic toad and spiny eel

Linghui Li[a,b,c,1], Yan Chai[a,1], Weiyu Peng[d,1], Delin Li[e,f], Litao Sun[g], George Fu Gao[a,b,2], Jianxun Qi[a], Haixia Xiao[f], William Jun Liu[h], Mark von Itzstein[c], and Feng Gao[f,i,2]

Contributed by George Fu Gao; received July 12, 2022; accepted September 2, 2022; reviewed by Pablo Guardado Calvo, Florian Krammer, and Rino Rappuoli

Influenza virus neuraminidase (NA) is an important target for antiviral development because it plays a crucial role in releasing newly assembled viruses. Two unique influenza-like virus genomes were recently reported in the Wuhan Asiatic toad and Wuhan spiny eel. Their NA genes appear to be highly divergent from all known influenza NAs, raising key questions as to whether the Asiatic toad influenza-like virus NA (tNA) and spiny eel NA (eNA) have canonical NA activities and structures and whether they show sensitivity to NA inhibitors (NAIs). Here, we found that both tNA and eNA have neuraminidase activities. A detailed structural analysis revealed that tNA and eNA present similar overall structures to currently known NAs, with a conserved calcium binding site. Inhibition assays indicated that tNA is resistant to NAIs, while eNA is still sensitive to NAIs. E119 is conserved in canonical NAs. The P119E substitution in tNA can restore sensitivity to NAIs, and, in contrast, the E119P substitution in eNA decreased its sensitivity to NAIs. The structures of NA–inhibitor complexes further provide a detailed insight into NA–inhibitor interactions at the atomic level. Moreover, tNA and eNA have unique N-glycosylation sites compared with canonical NAs. Collectively, the structural features, NA activities, and sensitivities to NAIs suggest that fish- and amphibian-derived influenza-like viruses may circulate in these vertebrates. More attention should be paid to these influenza-like viruses because their NA molecules may play roles in the emergence of NAI resistance.

Wuhan Asiatic toad influenza-like virus | Wuhan spiny eel influenza-like virus | neuraminidase (NA) | drug resistance | crystal structures

Significance

Neuraminidase (NA) is a good target for antiviral drugs due to its function of releasing progeny viruses. Recently, two influenza-like virus genomes derived from Asiatic toad and spiny eel were discovered. They appear to be highly divergent from all known influenza NAs, raising key questions about whether tNA and eNA have canonical activities and can be inhibited by NA inhibitors (NAIs). Here, we demonstrated that these two NAs display canonical NA activities and overall structures. However, eNA is sensitive to NAIs, while tNA is highly resistant to multiple NAIs. We found that residue 119 is the key amino acid that determines sensitivity to NAIs and further illustrated the drug-resistance mechanism by solving the high-resolution crystal structures of NA–NAI complexes.

Influenza virus is a significant contagious pathogen that causes severe or mild respiratory illness in humans worldwide. Influenza viruses are divided into four distinct types: A, B, C, and D (1). Influenza A viruses (IAVs) are further divided into subtypes based on the virus's two surface glycoproteins, hemagglutinin (HA) and neuraminidase (NA), and are the major cause of human pandemics, of which the main natural host is waterfowl. Additionally, IAVs infect a wide variety of mammalian and avian species, including humans, land birds, poultry, horses, pigs, dogs, cats, and some sea mammals (2–4). Notably, the genomes of some novel subtypes, for example H17N10 and H18N11, were discovered in bats in South America (5, 6). Recombinant H17N10 and H18N11 viruses have been generated by reverse genetics, and mammal-adapting amino acid substitutions were detected in the NA-like protein during passages in Madin–Darby canine kidney II cells, thereby enhancing viral replicative ability and conferring a broader tissue tropism in mice and ferrets (7, 8).

A 2018 study discovered 214 new vertebrate-associated RNA viruses by using a large-scale metatranscriptomic approach (9). Wuhan Asiatic toad and Wuhan spiny eel influenza-like viruses are two examples of novel influenza-like viruses that were first found in fish and amphibians (9). Six segments (PB1, PB2, PA, N, HA, and NA) and eight segments (PB1, PB2, PA, N, HA, NA, M, and NS) were identified in the Wuhan Asiatic toad and Wuhan spiny eel influenza virus genomes, respectively. Sequence alignment of the coding regions indicates that these two viral genomes display the closest hits to the influenza B virus (IBV) species. The percentage identity between Wuhan Asiatic toad and IBV ranges from 29 to 46%, while the percentage identity between Wuhan spiny eel and IBV ranges from 34 to 76%. Asiatic toad influenza-like virus NA (tNA) and spiny eel NA (eNA) have 35 and 48% amino acid identities to the IBV NA, respectively. Arunkumar et al. reported that the Wuhan spiny eel influenza virus NA-like protein has sialidase activity and is sensitive to NA inhibitors (NAIs) (10). Recently, Parry et al. identified two amphibian influenza-like viruses, which exhibit relatively high pairwise amino acid identity to segments from the influenza D virus genome (11). All of these findings suggest that there are perhaps a very large number of

Author contributions: F.G. designed research; L.L., W.P., and F.G. performed research; D.L., J.Q., and W.J.L. contributed new reagents/analytic tools; Y.C., L.S., G.F.G., H.X., M.v.I., and F.G. analyzed data; G.F.G. and F.G. wrote the paper; and M.v.I. revised the paper.

Reviewers: P.G.C., Institut Pasteur; F.K., Icahn School of Medicine at Mount Sinai; and R.R., Toscana Life Sciences Foundation.

The authors declare no competing interest.

[1]L.L., Y.C., and W.P. contributed equally to this work.

[2]To whom correspondence may be addressed. Email: gaof@im.ac.cn or gaofeng@tib.cas.cn.

This article contains supporting information online at http://www.pnas.org/lookup/suppl/doi:10.1073/pnas.2210724119/-/DCSupplemental.

Published October 3, 2022.

unknown influenza-like viruses, and our understanding of the origin, evolution, and cross-species transmission of these viruses is limited. Further, the zoonotic potential of these influenza-like viruses remains to be determined.

The viral surface glycoprotein NA plays critical roles in the life cycle of the influenza virus. For IAVs and IBVs, NA cleaves the glycosidic linkage between the capping sialic acids associated with host cell receptors to facilitate release of virion progeny away from infected cells and consequently prevents virus aggregation at the infected cell surface (12–14). Based on the NA sequence, classic NAs of IAVs are classified into two groups: group 1 (N1, N4, N5, and N8) and group 2 (N2, N3, N6, N7, and N9) (15–17). Two bat influenza-like virus NA-like proteins (N10 and N11) show structural similarity to the classic IAV NAs, to a certain extent, but lack the putative active site and do not have neuraminidase activity (6, 18, 19), indicating the complexity of viral NA structures.

High-resolution NA structures provide precise target information for drug design (20–22). The current clinically used antiinfluenza NAIs, zanamivir and oseltamivir carboxylate, were designed based on NA structures (23, 24). Although current drugs are generally efficient against most IAV and IBV strains, drug-resistant viruses can and do rapidly emerge. Characterization of the structures of new genetically divergent NAs and drug-resistant NAs will be important for the ongoing development of novel antiinfluenza drugs.

Currently, the NA function of most genetically distinct influenza-like viruses is unknown. To better understand the complexity and divergence of influenza virus NAs, we report here the functional and structural characterization of the NA protein of Asiatic toad and Wuhan spiny eel influenza-like viruses. We found that tNA and eNA have neuraminidase activities. Unexpectedly, however, tNA displayed a high resistance to clinically used NAIs (zanamivir, oseltamivir carboxylate, and peramivir), while eNA was still sensitive to NAIs. Both NAs share similarity in overall structural features when compared with other IAV and IBV NAs. Comparison of the framework residues and catalytic residues around the active site indicates that P119 (N2 numbering) in tNA is the only different amino acid among all NAs, which encode E119. Inhibition assays demonstrated that tNA with a P119E substitution displays increased sensitivity to NAIs, while eNA with an E119P substitution displays decreased sensitivity to NAIs. Analysis of the complex structures of NAs and inhibitors suggests that residue 119 is the critical amino acid that leads to tNA NAI resistance.

Results

Similar Overall Structures of tNA and eNA to Canonical NAs. Phylogenetic tree analysis indicated that tNA and eNA are more closely related to IBV than IAV (Fig. 1*A* and *SI Appendix*, Table S1). The crystal structures of the tNA and eNA ectodomains were determined at resolutions of 2.0 and 2.4 Å, respectively (*SI Appendix*, Tables S2 and S3). The overall structures of these two NAs are highly similar to other known influenza virus NA structures, despite sequence identities as low as ∼40%. The crystal structures of tNA and eNA reveal a canonical "mushroom-shaped" tetramer assembled with four identical monomer heads consisting of a propeller-like arrangement of six four-stranded β-sheets, as described previously for other IAV and IBV NAs (Fig. 1*B*) (25). The active site is located at the center of each monomer. Comprehensive structural alignment among tNA, eNA, IBV, and representative influenza A N1 to N11 subtypes revealed rmsd's ranging from 0.96 to 2.00 Å for Cα atoms of single NA monomers (*SI Appendix*, Table S1). tNA and eNA are more structurally similar to IBV NAs, with moderately lower rmsd's of 1.37 and 0.96 Å, respectively. The structural alignment and sequence identities are in line with the phylogenetic analysis, suggesting that tNA and eNA are more closely related to IBV than IAV NAs.

Unique Framework Residues in tNA and eNA. Residues within the active site are highly conserved among all typical IAV and IBV NA subtypes, including eight charged and polar residues that directly interact with the substrate at the catalytic site (R118, D151, R152, R224, E276, R292, R371, and Y406). The geometry of the catalytic site is supported through a network of hydrogen bonds and van der Waals forces by 11 conserved framework residues (E119, R156, W178, S179, D/N198, I222, E227, H274, E277, N294, and E425) (26, 27). Comparison of tNA with 09N1 (the NA of A/California/04/2009 H1N1) and IBV NA structures shows a remarkable similarity, both in the general fold and in the spatial arrangement of the catalytic residues (Fig. 1 *C* and *D*). The residues and conformation of the active sites and framework of tNA are virtually identical to that of typical IAV and IBV NAs, except for framework residues 119 and 274 (Fig. 1*E*). In typical NAs, these two highly conserved residues are glutamic acid and histidine, whereas in tNA, those residues are proline and methionine, respectively, which have not been identified in other naturally occurring NAs to our knowledge. In previous studies, mutations at residues E119 and H274 were thought to lead to drug resistance (28–34). With these two critical substitutions, we hypothesized that tNA might not be as susceptible to NAIs as typical NAs. For eNA, M274 is the only different framework residue between eNA and other canonical NAs.

Comprehensive Analysis of Influenza Virus NA Loop Variations. By overlapping the structures of tNA and eNA with the representative A-type NA N1 to N9 subtypes and the IBV NA, we found that the structures of all NA subtypes exhibit different conformations of the 150-, 270-, 340-, 290-, and 430-loops (Fig. 2*A*). The 150-loop has a very flexible conformation and high diversity in different NA subtypes. The 150-loop in the tNA and eNA structures adopts a very similar conformation to the IAV group 2 NAs and the IBV NA's closed conformation. Sequence alignment of the amino acids of the 150-loop segment (146 to 152) suggests that residue 149 plays an important role in regulating the 150-loop conformation, as previously described in other studies (35). Residue 149 is a valine in group 1 NAs with an opened 150-loop, whereas it is an isoleucine or arginine in group 2 and IBV NAs with a closed 150-loop. In IBV NA, the bulky guanidino side chain of the conserved R149 makes interactions with D429, contributing to the relative stability of both the 150- and 430-loops (Fig. 2*B*). In tNA, G149 loses the interaction with residues on the 430-loop, leading the 430-loop to shift away in the opposite direction from the active site. The interactions between K432 with L471 and L472 further fix the 430-loop. W149 in eNA forms a π–π interaction with Q433 in the 430-loop, yielding a closer distance between the 150- and 430-loops compared with IBV NA (Fig. 2*E*). Although residue 150 in the eNA, tNA, and IBV NAs is not identical, the interactions between residue 150 and H136 exist in these NAs, which keeps the 150-loop in a closed conformation. Also, the guanidino group of R152 makes an interaction with the side chain of D198, as has been observed in these three NAs (Fig. 2 *B* and *E*).

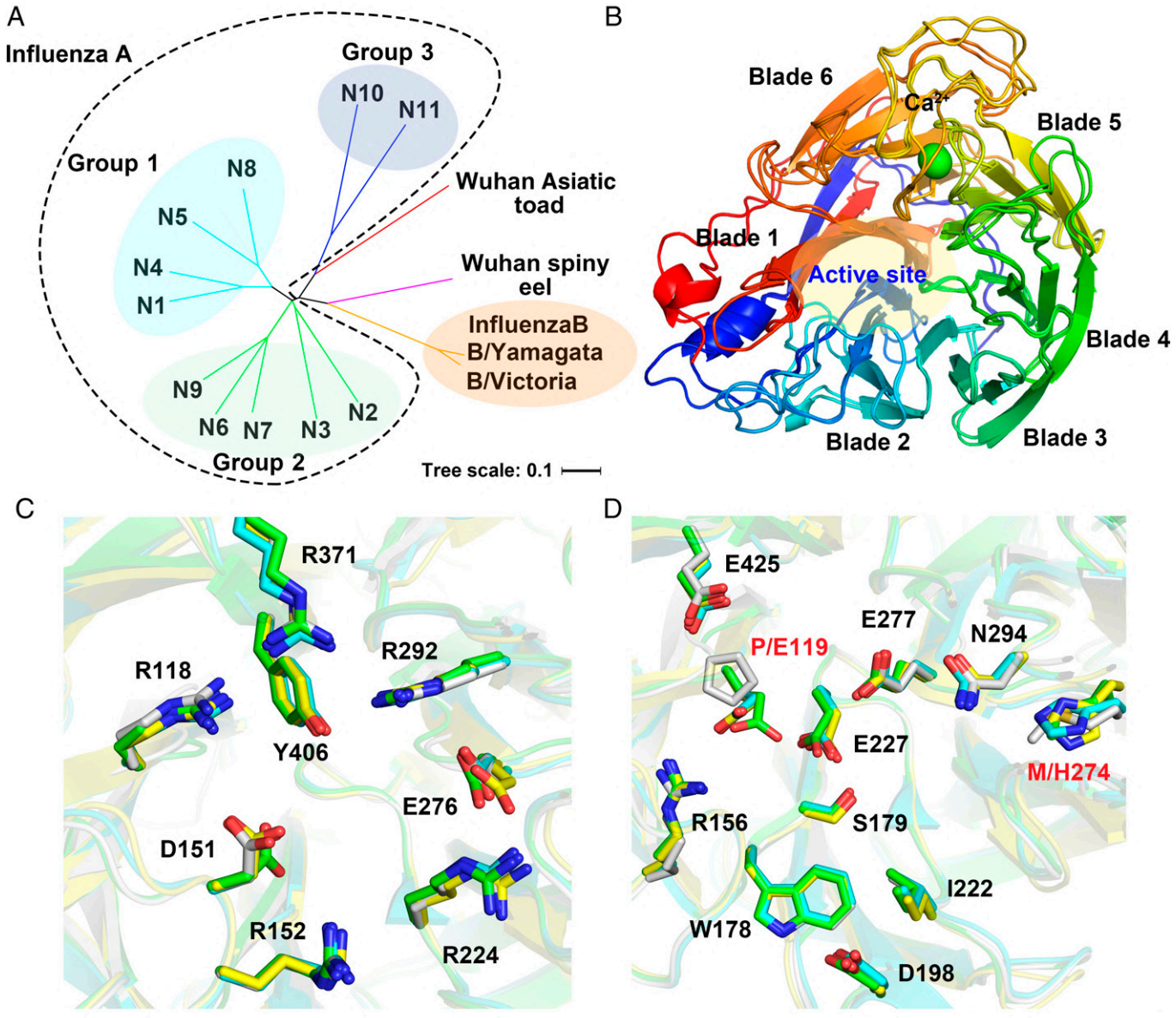

E

Subtype	Catalytic site residues								Framework residues										
	118	151	152	224	276	292	371	406	119	156	178	179	198	222	227	274	277	294	425
N1-N9	R	D	R	R	E	R	R	Y	E	R	W	S	N/D	I	E	H	E	N	E
Influenza B NA	R	D	R	R	E	R	R	Y	E	R	W	S	D	I	E	H	E	N	E
Toad NA	R	D	R	R	E	R	R	Y	P	R	W	S	D	I	E	M	E	N	E
Eel NA	R	D	R	R	E	R	R	Y	E	R	W	S	D	I	E	M	E	N	E

Fig. 1. Phylogenetic analyses of tNA, eNA, and representative IAV and IBV NAs and overall structures of tNA and eNA with a conserved active site. (*A*) Phylogenetic analyses of tNA, eNA, and representative IAV and IBV NA genes. IAV NAs fall into two distinct groups: group 1 and group 2, shaded in cyan and green, respectively. The bat-derived N10 and N11 were grouped as influenza A–like group 3, colored in purple. IBV NA B/Yamagata-like and B/Victoria-like NAs are in orange. (*B*) NA monomers viewed from the top of the molecule are shown as a ribbon representation to illustrate the canonical β-propeller arrangement with six four-stranded β-sheets. A conserved single bound calcium ion is shown as a green sphere. The putative active-site region at the center of the six-bladed β-propeller structure is highlighted and colored in yellow. (*C* and *D*) Comparison of the catalytic-site and framework residues in tNA (gray), eNA (black), IAV N1 (PDB ID code 2HTY; yellow), and IBV NA (PDB ID code 4CPL; cyan). The same coloring scheme is used in subsequent figures. The residues at the active site of tNA that are conserved in NAs are labeled in black, whereas the substituted residues are labeled in red. (*E*) Sequence alignment shows all 8 key catalytic-site residues are conserved, 2 of 11 framework residues are substituted in tNA, and 1 of 11 framework residues is substituted in eNA.

Compared with other NA subtypes, tNA shows a high diversity at residues 271 to 275 of the 270-loop. Whereas all IAV NAs of group 1 orient to the left, tNA and eNA are similar to IBV and group 2 IAV NAs, which are directed to the right (Fig. 2*A*). The terminal nitrogen atom of the K251 side chain of tNA forms hydrogen-bond interactions with the side chains of S272 and S269. The side chain of S273 makes a polar interaction with Y316 (Fig. 2*C*). In the 270-loop of IBV NA, the guanidino group of the R271 side chain makes hydrogen-bond interactions with N340, D293, and a water molecule, helping

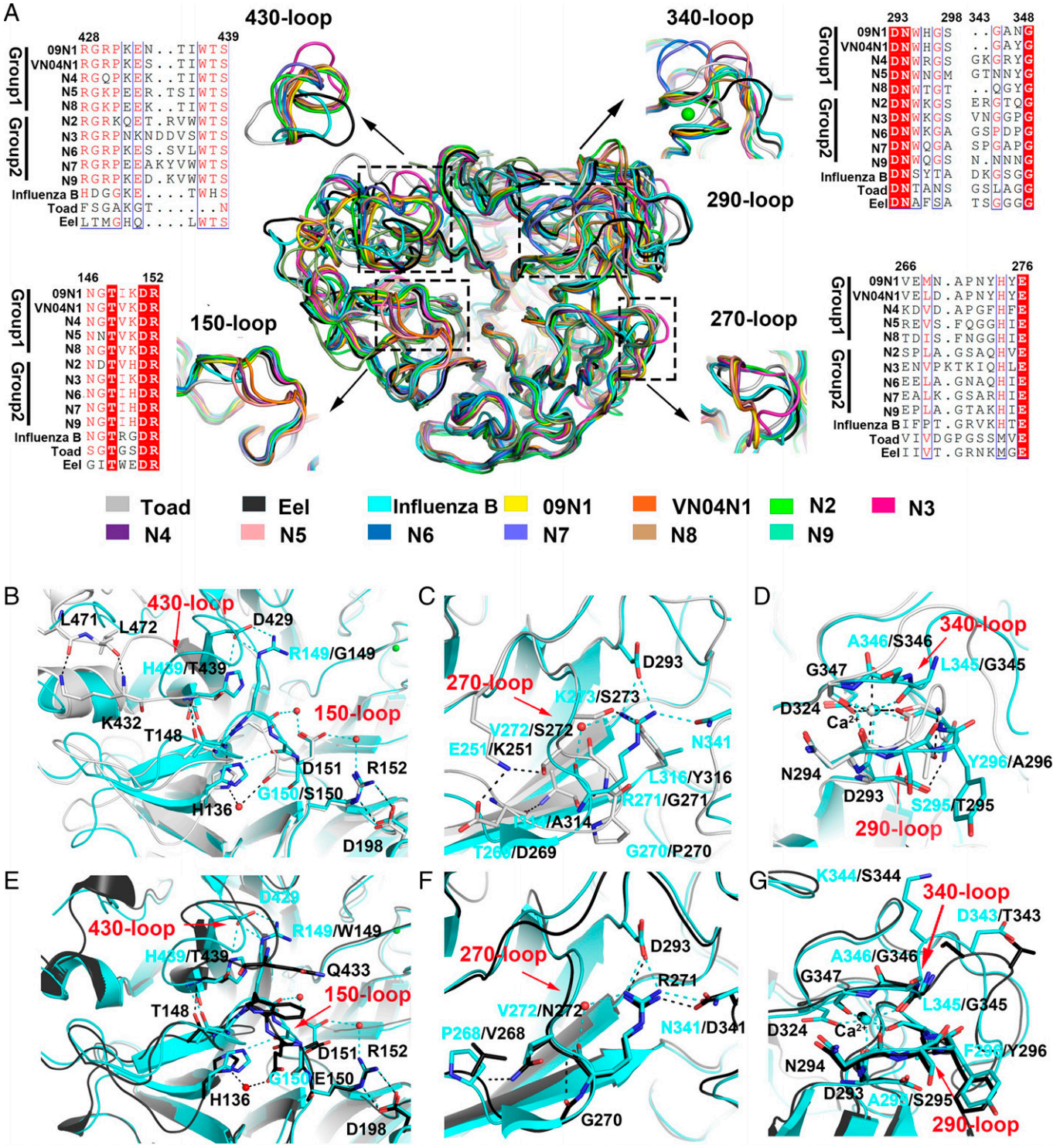

Fig. 2. Comparison of the variable 150-, 270-, 290-, 340-, and 430-loops among tNA, eNA, and all typical IAV and IBV NA subtypes. (*A*) Structures of 09N1 (PDB ID code 3NSS), VN04N1 (PDB ID code 2HTY), N2 (PDB ID code 1IVG), N3 (PDB ID code 4HZV), N4 (PDB ID code 2HTV), N5 (PDB ID code 3SAL), N6 (PDB ID code 4QN4), N7 (PDB ID code 4QN3), N8 (PDB ID code 3O9J), N9 (PDB ID code 7NN9), IBV NA (PDB ID code 4CPL), tNA (PDB ID code 7FGB), and eNA (PDB ID code 7XVR) are superimposed and shown in cartoon representation. The loops are highlighted and detailed in the panels with multiple-sequence alignment of these regions from all NA subtypes generated in ESPript 3.0. (*B*–*D*) Comparison of the detailed polar interactions involved in the 430-, 290-, 150-, 270-, and 340-loops between tNA and IBV NA. (*E*–*G*) Comparison of the detailed polar interactions involved in the 430-, 290-, 150-, 270-, and 340-loops between eNA and IBV NA.

to stabilize the 270-loop conformation. The 270-loop in eNA displays a similar conformation to IBV NA, mainly due to the identical R271 residue (Fig. 2*F*).

The 340- and 290-loops constitute the binding site of a highly conserved calcium ion. Compared with the other NA subtypes, the tNA 340-loop is directed away from the conserved calcium ion, while the 290-loop is relatively closer to the conserved calcium ion. Despite these differences, the two loops still maintain coordination with the calcium ion, and this may be related to the amino acid substitution of residue 295. In IAV NAs, residue 295 is a conserved tryptophan and an asparagine in IBV NA that cannot interact with the calcium ion (Fig. 2*D*). In tNA, residue

295 is a threonine, and the main-chain carbonyl oxygen coordinates with the calcium ion, drawing the 290-loop closer to the calcium ion. The side chain of T295 forms a hydrogen bond with the side chain of D293, yielding a relatively stable 290-loop conformation. In addition, residue G347 on the 340-loop interacts with the backbone carbonyl oxygen of N294, which keeps the distance between the 340-loop and the 290-loop relatively stable (Fig. 2*D*). For eNA, the conformation of the 290- and 340-loops displays higher similarity to IBV NA than tNA (Fig. 2*G*).

Conserved Calcium Ion Binding Site. The calcium ion is important for the thermostability and catalytic activity of influenza NAs (36, 37). One conserved calcium ion binding site found in all known IAV and IBV NAs was also observed in tNA and eNA. Five residues and one water molecule coordinate with the calcium in IAV and IBV NAs (Fig. 3 *A* and *B*). In tNA, the calcium binding site is formed by four backbone carboxyl oxygens from D293, T295, N297, and G347, one of the carboxyl oxygens from D324, and a water molecule. Among these interactions, D324, D293, and the water molecule are conserved in IAV NAs, IBV NA, and tNA. Residue 295 in tNA replaces residue 345 in both IAV and IBV NAs, forming interactions with the calcium ion (Fig. 3*C*). In eNA, four of six residues are identical to IBV NA, but residue 295 is replaced with alanine (Fig. 3*D*).

In previous studies, another two potential calcium binding sites were observed in N1 subtypes. One of the calcium ions is located at the fourfold axis of the NA tetramer, which is observed in the 1918 H1N1 (A/Brevig Mission/1/18), CA09 H1N1 (A/California/04/2009), and H5N1 (A/Vietnam/1203/04) NAs (16, 35, 38). The other putative calcium binding site is closely located by the 380-loop in 18N1 and IBV NAs. However, there is no strong electron density around these two potential calcium ion binding sites in either tNA or eNA.

Unique Glycosylation Sites. The ectodomain of tNA possesses five putative N-glycosylation sites at N54, N55, N75, N234, and N329. The tNA construct contains residues 80 to 466, including two putative glycosylation sites. Due to the poor occupancy, only one glycan molecule is observed at N234, which is also found in other influenza NAs. In contrast, the eNA ectodomain has two putative N-glycosylation sites (N48 and N283), and only N283 is involved in the construct. As expected, glycan density can be observed at N283. Unexpectedly, both tNA and eNA lack a potential N-glycosylation site at position 146, which is conserved in other influenza virus A and B NAs and is located close to the substrate binding site (39). N-glycosylation is predicted to occur at asparagine residues in the N-X-S/T consensus sequence motif of a protein, in which X denotes any amino acid except P (40). In tNA and eNA, the conserved N146 is mutated to S146 and G146, respectively, indicating that there are no N-glycosylation sites. The absence of glycan electronic density at residue 146 further confirms this hypothesis (Fig. 4).

Neuraminidase Activity and Sensitivity to Multiple NAIs. To investigate whether the genetically divergent tNA and eNA have canonical neuraminidase activities, we determined the Michaelis constants (K_ms) of soluble recombinant tNA, eNA, IAV NA

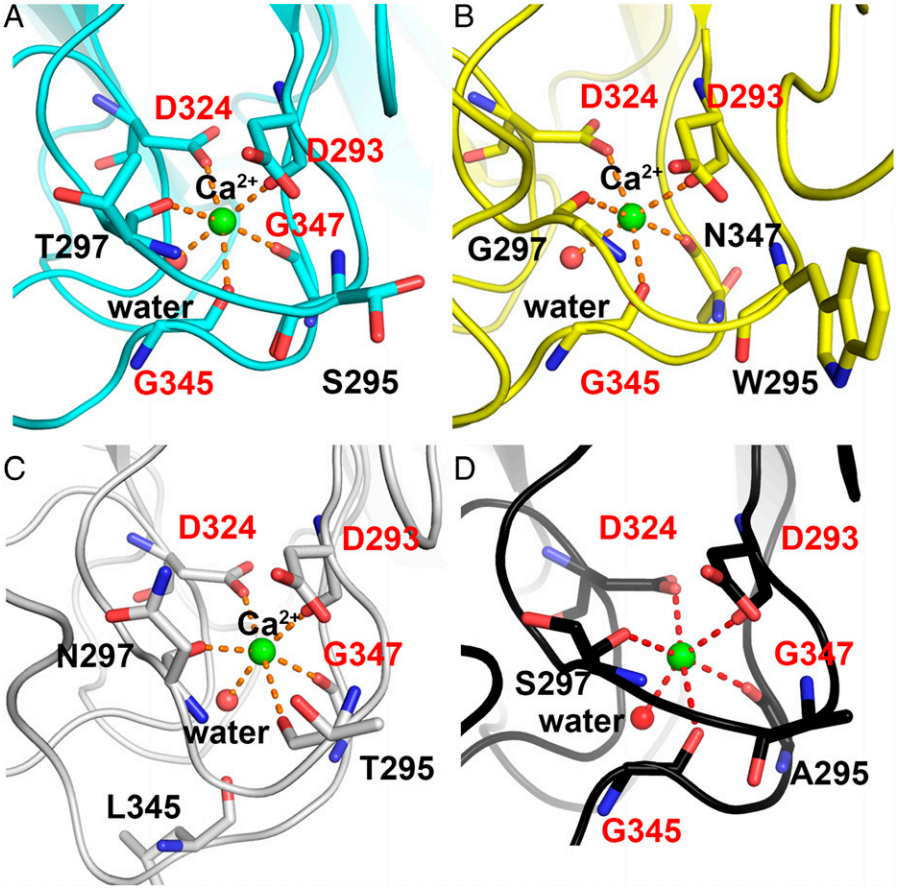

Fig. 3. Comparison of the highly conserved calcium binding site of tNA, eNA, 09N1, and IBV NA. One calcium ion binding site was observed in tNA, which is conserved in all known NAs from IAV and IBV. The calcium ion is shown as a green sphere, and the water molecule coordinated with the calcium is shown as a red sphere. Residues interacting directly with the calcium are shown as sticks. Interactions between calcium and coordinating residues are shown in orange. Among IBV NA (*A*; cyan), 09N1 (*B*; yellow), tNA (*C*; gray), and eNA (*D*; black), conserved calcium-coordinating residues are labeled in red.

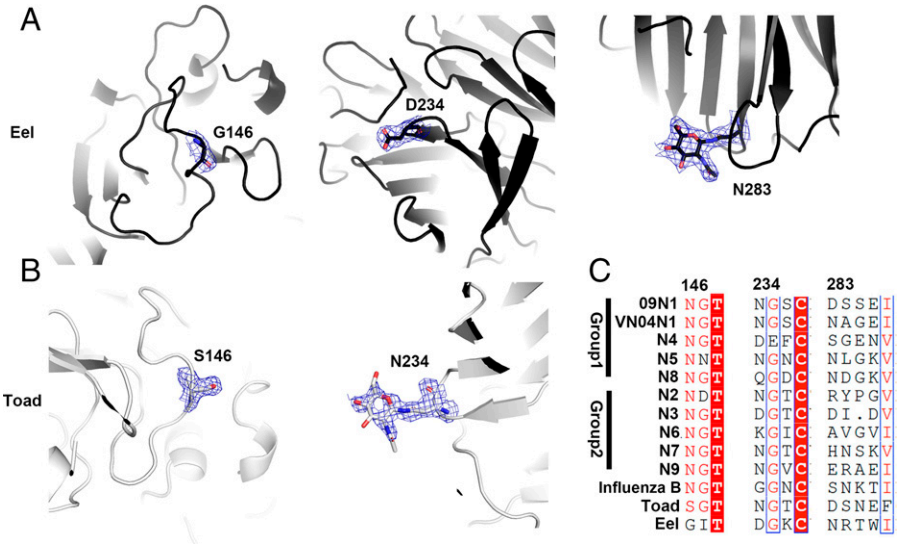

Fig. 4. N-linked glycosylation analysis between eNA and tNA. (*A*) The density map of residues 146, 234, and 283 in eNA. One glycan can be observed at N283. (*B*) The density map of residues 146 and 234 in tNA. (*C*) Sequence alignment of sites among N1 to N9, IBV, eNA, and tNA referenced in *A* and *B*. The residues and glycans of eNA and tNA are shown as black and gray sticks, respectively. The s*A*-weighted $2F_o - F_c$ electron density maps of the glycans and residues are contoured at 0.5 σ.

(09N1), and IBV NA using a standard 4-MUNANA–based fluorescence assay and determined values of 45.35, 6.91, 26.12, and 8.14 μM, respectively (Table 1). These data indicate that tNA and eNA are functionally comparable to other influenza virus NAs. Compared with typical influenza NAs, tNA displayed a slightly lower affinity for the substrate, with a 1.7- and 5.6-fold reduced K_m relative to 09N1 and IBV NA, respectively. The decreased enzymatic activity of tNA may be related to the substitution of the key residue E119 in the active site, which interacts with the substrate. In contrast, eNA which contains E119 displayed comparable affinity to 09N1 and IBV NA for the substrate.

To explore the susceptibility of tNA and eNA to current widely clinically used NAIs, the 50% inhibitory concentration (IC_{50}) of three NAIs (zanamivir, oseltamivir carboxylate, and peramivir) was determined using the same fluorescence-based assay (Table 1 and *SI Appendix*, Fig. S1). In line with previous findings, zanamivir, oseltamivir carboxylate, and peramivir inhibited N1 and IBV NA with potencies in the range of 0.43 to 0.83 and 5.22 to 16.88 nM, respectively. In contrast, highly reduced sensitivity of tNA to these three NAIs was observed, with IC_{50} values of 141 nM, 10.4 μM, and 1.7 μM, respectively. Remarkably, the tNA protein displayed extreme resistance to oseltamivir carboxylate (12,503- and 683-fold reduction compared with 09N1 and IBV NA, respectively). In the case of zanamivir, tNA conferred less resistance relative to oseltamivir carboxylate (328- and 27-fold reduction compared with N1 and IBV NA, respectively). Thus, tNA demonstrated an intermediate degree of drug resistance to peramivir, a cyclopentane derivative containing an oseltamivir-based 3-pentyloxy group in combination with a zanamivir-based 4-guanidino group, compared with zanamivir and oseltamivir carboxylate. In contrast, eNA exhibited sensitivity to all three tested NAIs. Therefore, we conclude that the tNA and eNA proteins have biologically relevant neuraminidase activities. eNA is sensitive to multiple NAIs, while tNA shows differences in the degree of cross-resistance to NAIs.

Sequence alignment indicates that residue 119 is the only amino acid different between the framework and catalytic residues of tNA and eNA. To determine if residue 119 is the key site resulting in drug resistance, tNA-P119E and eNA-E119P proteins were expressed and purified to perform inhibition assays. Compared with tNA, the IC_{50} values of tNA-P119E for zanamivir, oseltamivir carboxylate, and peramivir decreased 20.6-, 16.3-, and 42-fold, respectively. In contrast, eNA-E119P displayed increased resistance to zanamivir, oseltamivir carboxylate, and peramivir by 14.1-, 5.10-, and 7.1-fold, respectively (Table 1 and *SI Appendix*, Fig. S1).

Table 1. Enzyme kinetic parameters of Wuhan Asiatic toad NA, Wuhan spiny eel NA, 09N1, and IBV NA and inhibitory susceptibility of three NA inhibitors

	IC_{50} ± SEM, nM*			Kinetic parameters†
NA subtype	Zanamivir	Oseltamivir carboxylate	Peramivir	K_m ± SEM, μM
A/California/04/2009 (H1N1)	0.43 ± 0.06	0.83 ± 0.18	0.45 ± 0.08	26.12 ± 1.79
B/Singapore/222/1979	5.22 ± 1.44	15.21 ± 3.00	16.88 ± 1.94	8.14 ± 0.84
Wuhan Asiatic toad NA	140.90 ± 17.50	10,378 ± 594	1,731 ± 231	45.35 ± 5.41
Wuhan Asiatic toad NA-P119E	6.83 ± 2.01	637.50 ± 122.88	41.23 ± 19.74	107.99 ± 10.03
Wuhan spiny eel NA	8.37 ± 3.68	13.85 ± 1.73	1.55 ± 0.21	6.91 ± 0.31
Wuhan spiny eel NA-E119P	117.71 ± 33.17	70.55 ± 18.16	10.99 ± 4.98	17.28 ± 1.19

*The IC_{50} value is the half-maximal inhibitory concentration against the influenza virus neuraminidase. Data shown are the mean ± SEM of three independent experiments.
†The enzyme kinetic data were fitted to the Michaelis–Menten equation by nonlinear regression to determine the Michaelis constant (K_m) using GraphPad Prism 7. Values are the mean ± SEM from three independent experiments, done in triplicate.

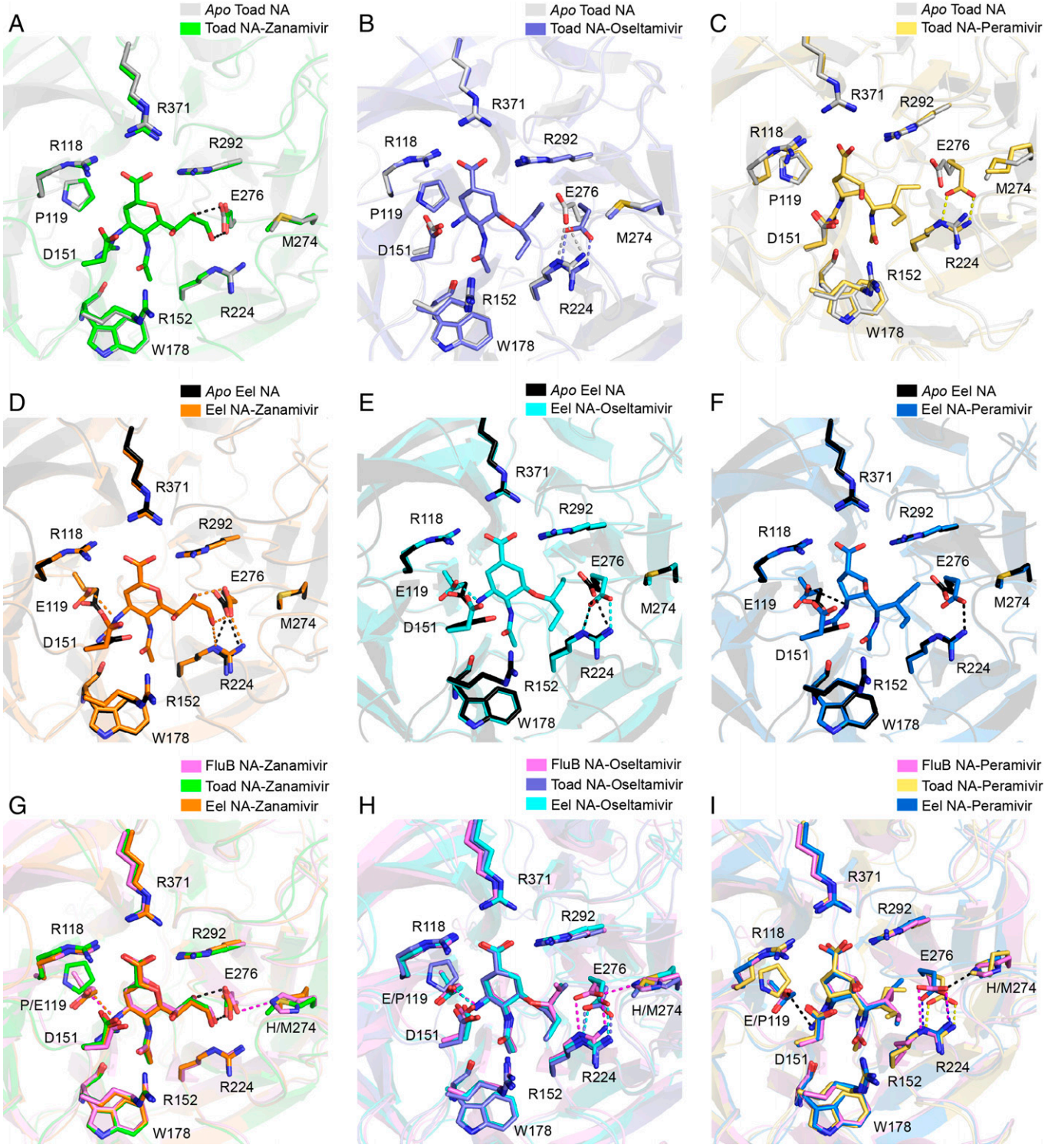

Fig. 5. Structural basis of sensitivity of eNA and antiviral resistance mechanism of tNA. (*A–C*) Comparison of the active site of apo tNA and with bound inhibitors. The key interaction residues at the active site of tNA are shown as sticks. (*D–F*) Comparison of the active site of apo eNA and with bound inhibitors. The key interaction residues at the active site of eNA are shown as sticks. (*G–I*) Comparison of the binding modes of zanamivir, oseltamivir carboxylate, and peramivir in complex with tNA, eNA, and IBV NA. The hydrogen-bond interactions involved in the specific substitutions E119P and H274M are shown as dashed lines. NAs are shown with bound inhibitors similarly colored. Structures of apo IBV (PDB ID code 4CPL), IBV-oseltamivir (PDB ID code 4CPM), IBV-zanamivir (PDB ID code 4CPN), and IBV-peramivir (PDB ID code 3K37) are shown in cartoon representation.

The Structural Basis for tNA Drug Resistance. To gain insight into the structural basis of the multidrug resistance of tNA, we determined the crystal structures of tNA in complex with zanamivir, oseltamivir carboxylate, and peramivir, respectively, by soaking the three NAIs into the apo tNA crystals. The structures of tNA–inhibitor and eNA–inhibitor complexes were determined at resolutions from 1.6 to 2.8 Å (*SI Appendix*, Tables S2 and S3). Zanamivir, oseltamivir carboxylate, and peramivir share two identical functional groups (carboxylate and acetamido groups), making similar interactions with conserved residues in the tNA or eNA active site (Fig. 5). The conserved carboxyl moiety at C1 of these inhibitors makes an electrostatic

interaction with the highly conserved triarginyl cluster (R118, R292, and R371). The acetamido substituent of these three inhibitors makes hydrogen-bond interactions with E227 and R152 through its amide NH and carbonyl group, respectively. The methyl group of the acetamido substituent is also well-accommodated in the hydrophobic pocket formed by W178, I222, and the aliphatic moieties of R152 and R224, typical of these inhibitors when in complex with other influenza virus NAs (Fig. 5 *A*–*C*). Superimposing the unbound apo tNA with the tNA–zanamivir complex structure, we found that the conformations of all key residues that interact with the inhibitor are virtually identical. However, in tNA structures in complex with oseltamivir carboxylate and peramivir, which share a hydrophobic pentyl ether group replacing the glycerol side chain of zanamivir, E276 rearranges to form a salt bridge with the R224 side chain (Fig. 5 *B* and *C*). This conformational change has also been found in various IAV and IBV NAs (16, 41–43). Comparison of apo eNA with eNA–NAI complex structures revealed that the side chains of E119, D151, and E276 orientate to the active site in the apo eNA structure (Fig. 5 *D*–*F*).

The inhibition assay data indicate that residue 119 plays an important role in NA sensitivity to NAIs. Comparison of the tNA–zanamivir and eNA–zanamivir complexes with IBV NA–zanamivir complexes revealed that E119 is critically involved in interactions with the positively charged guanidino group of zanamivir and peramivir, and with the corresponding amino group of oseltamivir carboxylate, as observed in other typical influenza virus NAs (Fig. 5 *G*–*I*). In contrast, P119 in tNA is a neutral amino acid, which bears a shorter side chain. Consequently, P119 cannot form electrostatic interactions with the guanidino or amino group of zanamivir, peramivir, or oseltamivir carboxylate, resulting in a decrease in the binding affinity of tNA to NAIs. This readily explains why tNA shows resistance to all three inhibitors (Fig. 5 *G*–*I*).

It is worth noting that tNA exhibited different levels of resistance to the three inhibitors, with the order of resistance from strongest to lowest resistance being oseltamivir carboxylate > peramivir > zanamivir. The structures of NA–inhibitor complexes were further analyzed to provide an explanation for this order of drug resistance. The C4 position of oseltamivir carboxylate bears an amino group, which interacts with the side chains of E119 and D151 and two water molecules in IAV NAs. Due to the E119P substitution in tNA, only the interaction between the amino group of oseltamivir carboxylate and residue D151 remains. In the tNA E119P substitution mutant, while zanamivir and peramivir also lose the salt bridge between residue E119 and the guanidino group, they still retain the interactions with E227, W178, and D151 through the bulkier guanidino group, which indicates that E119P will be better tolerated by zanamivir and peramivir than oseltamivir carboxylate.

For residue 274, located on the other side of the active site, both tNA and eNA have a nonpolar methionine compared with a positively charged histidine in canonical NAs. M274 impacts little on the conformation of the E276 side chain in the zanamivir binding structures but leads to the adoption of a nonoptimal conformation of the hydrophobic pentyloxy group in both oseltamivir carboxylate and peramivir (Fig. 5 *G*–*I*). In the complex structures of IBV NA–NAIs, E276 can form hydrophobic interactions with the side chain of E274 in addition to the interactions with the side chain of R224. In contrast, E276 loses the interaction with M274 and forms hydrophobic interactions with the side chain of R224. The conformation of the residues around the glycerol group of zanamivir and pentyloxy group of oseltamivir carboxylate/peramivir displays little difference between tNA and eNA. Therefore, M276 is not the key residue related to drug resistance.

In summary, the E119P substitution prevents interaction with the guanidino group of zanamivir and peramivir and the amino group of oseltamivir carboxylate, which leads to the antiviral resistance of tNA.

Discussion

To explore the characterization of influenza-like virus NA from amphibia and fish, we generated high-purity tNA and eNA using the baculovirus expression system. It is interesting to note that these two NAs have the same neuraminidase activity as typical influenza NAs. However, they exhibit different sensitivities to multiple NAIs at the protein level. eNA was sensitive to zanamivir, oseltamivir carboxylate, and peramivir, while tNA was resistant to three NAIs, particularly to oseltamivir carboxylate (>10,000-fold reduced sensitivity compared with canonical N1). Sequence alignment indicates that among framework residues and catalytic residues, residue 119 is the only difference between tNA and eNA. The E119P mutation in tNA led to resistance to NAIs, and P119E in eNA increased sensitivity to NAIs. The structures of tNA complexed with NAIs further illustrate the molecular mechanism of drug resistance.

Influenza viruses are well-known to infect a broad spectrum of host species, including domestic and wild birds, pigs, horses, and dogs, with sporadic outbreaks in seals, whales, ferrets, and cats. However, there have been few studies of influenza-like viruses from amphibia and fish. Two NA-like molecules were identified in influenza-like genomes from bat specimens (5, 6). The amino acid sequence homology between these two bat IAV NAs compared with conventional NAs is <30%. They form a typical homotetrameric "box shape" complex, with each monomer containing a propeller-like structure of six antiparallel β-sheets in the head domain. However, they have much wider substrate binding site pockets, and the catalytic-site and framework residues are not conserved compared with canonical NAs, resulting in a lack of neuraminidase activity (6, 18, 19). In a recent study, NA genes were identified in toad and eel samples (9). Notably, tNA and eNA show the highest similarity to IBV NA, with sequence identities of 35 and 48%, respectively. While this is a relatively low sequence identity, these two NAs display highly similar overall structures to other typical influenza virus NAs with a conserved active site and a calcium binding site, indicating that tNA may facilitate the release of progeny virus. Moreover, it is possible that a real virus exists in nature, even though M and NS segments of Wuhan Asiatic toad influenza-like virus have not been identified. Our data clearly indicated that tNA is multiply drug-resistant to NAIs, particularly oseltamivir carboxylate and peramivir. It is indeed possible that drugs contaminate the toad's habitat and caused the emergence of virus escape mutants under selective pressure (*SI Appendix*, Fig. S2), which is an interesting hypothesis that needs to be addressed in the future. These influenza-like viruses may potentially circulate in vertebrates, and therefore they should be monitored. eNA is more sensitive to peramivir than to the other two NAIs, which is consistent with a previous report (10). This is probably due to peramivir containing an oseltamivir-based 3-pentyloxy group in combination with a zanamivir-based 4-guanidino group.

Seroepidemiological data indicate a high prevalence of H17- (38%) and H18- (50%) specific antibodies in various screened Central and South American bats, suggesting that infections with these viruses are not limited to individual bat species (6). Preliminary studies of bat-derived H18N11 influenza-like virus show that N11 does not have canonical neuraminidase activity and cannot be propagated in human cell lines (15). However,

its replication ability can be increased after accumulation of two mammal-adapting mutations in the NA-like protein (NA-F144C and NA-T342A) as a result of passaging the reverse genetics–generated H18N11 virus (8).

Because tNA and eNA have neuraminidase activities similar to typical influenza virus NAs, from the perspective of influenza-like virus NA, the new Wuhan Asiatic toad influenza-like virus genome and Wuhan spiny eel influenza virus genome have the potential to produce real influenza viruses in nature. In this regard, it will be interesting to investigate whether these two influenza-like virus genomes can be propagated by reverse genetics and infect mammalian cell lines or whether they need to undergo significant changes to infect and spread among human cells. A recent study reports that the HA of Wuhan spiny eel influenza-like virus can bind to a unique GM2 gangliosidic receptor, which is also an interacting partner for some reoviruses and rotaviruses (10). This study proves that eNA is a sialidase and is sensitive to NAIs, which is similar to our results reported here (10). Although no preexisting immunity or postvaccination-induced antibodies were detected against the HA or NA of Wuhan spiny eel influenza virus, we still cannot rule out the possibility that this virus has a mammalian or avian origin. Because toad influenza-like virus is also similar to IBV, it would be possible to rescue this virus by using M and NS segments with the other six genome segments of toad influenza-like virus. Moreover, it will also be interesting to perform a seroepidemiological investigation to explore which species may have the specific antibodies to tNA in nature.

The glycosylation of NA at residue N146 may be required for NA function because it is highly conserved in NAs from almost all influenza virus strains, regardless of the host. It is interesting to note that both tNA and eNA lack this glycosylation site. A similar phenomenon has also been observed in influenza A/WSN/33 virus. The N-glycan at this glycosylation site affects NA enzymatic activity and plays a key role in the neurovirulence of WSN virus mice (39). Moreover, substitution of N146 in N8 NA leads to a change in substrate preference, and abolishment of the N-glycosylation site at N146 of N8 NA does not affect its proper maturation and transport to the cell surface, suggesting that glycosylation at N146 is important for function rather than a structural requirement (37).

Taken together, in the current study, we demonstrated that the tNA and eNA proteins have canonical overall structures and functions comparable to other typical influenza virus NAs. Importantly, tNA is highly resistant to all current clinically used NAIs, particularly oseltamivir carboxylate and peramivir. In contrast, eNA maintained sensitivity to NAIs. Sequence alignment, inhibition assays with mutant proteins, and complex structures demonstrated that P119 in tNA plays an important role in resistance to anti–influenza virus drugs. These data suggest that the NA protein of the natural Wuhan Asiatic toad influenza-like virus genome has already acquired multiple NAI-resistant point mutations without known exposure to a drug. Our detailed structural studies of tNA provide insights into understanding the newly identified influenza NAs and underlining the mechanism of drug resistance.

Materials and Methods

Cloning, Expression, and Purification of NA Proteins. The ectodomain (residues 80 to 466, N2 numbering) of tNA from the Asiatic toad influenza virus (GenBank accession no. MG600049.1) and the ectodomain (residues 83 to 472, N2 numbering) of NA from Wuhan spiny eel (GenBank accession no. AVM87625.1) were expressed in a baculovirus system for functional and structural analyses, as described in our previous reports (43, 44–47). Briefly, for NA enzymatic assays, the protein was purified by Ni-affinity chromatography followed by size-exclusion chromatography. For the crystallization experiments, the NA proteins were digested with thrombin to remove the His tag and a vasodilator-stimulated phosphoprotein tetrameric tag. The cleaved NA proteins were further purified by size-exclusion chromatography. Purified 09N1 and IBV NA (B/Singapore/222/1979) proteins were prepared following the protocols as previously reported (35, 41).

Crystallization, Data Collection, and Structure Determination. Crystallization experiments were performed using the sitting-drop vapor-diffusion method with commercial kits (Hampton Research and Molecular Dynamics). Apo tNA crystals were obtained by mixing 1 μL of 8 mg/mL protein in 20 mM Tris and 50 mM NaCl (pH 8.0) with a 1-μL reservoir solution (0.2 M lithium sulfate monohydrate, 0.1 M sodium citrate tribasic dihydrate, pH 5.0, and 26% [volume (vol)/vol] polyethylene 200) at 293 K. Apo eNA crystals were obtained in 4.0 M potassium formate, 0.1 M bis-Tris propane (pH 9.0), and 2% (weight/vol) polyethylene glycol monomethyl ether 2,000. For inhibitor soaking, NA crystals were soaked in 10 mM zanamivir, oseltamivir carboxylate, or peramivir for 30 min. Apo and soaked NA crystals were cryoprotected in mother liquor with the addition of 20% (vol/vol) glycerol and flash-cooled at 100 K. Diffraction data for apo and inhibitor complex crystals were collected using beamlines BL17U1 and BL02U1 at the Shanghai Synchrotron Radiation Facility. Initially, diffraction data were processed and scaled using HKL-3000 (48) or XDS (49). After inspecting the diffraction images, we found the striking feature of a periodic sharp diffuse pattern of reflections and a large portion of extraneous electron density overlapping with the model after several rounds of refinement. An intrinsic problem associated within the tNA crystal represents a pathological imperfection, a so-called lattice-translocation defect (50), which was also observed in 1918 N1 (51). The intensity was corrected according to a previously established method with a translocation vector (1/2, 0, 1/2) (52). The apo tNA and apo eNA structures were solved by molecular replacement using the program MOLREP (53) with the structures of B/Lee/40 NA (Protein Data Bank [PDB] ID code 1B9S) and B/Perth/211/2001 NA (PDB ID code 3K36) as search models, respectively. The complex structures with inhibitors were subsequently determined using the refined tNA and eNA as input models. Initial rigid-body refinement and manual model building were performed with phenix.refine (54) and Coot (55), respectively. Further rounds of refinement were performed using the phenix.refine program implemented in the Phenix package (54). The stereochemical quality of the structures was analyzed using the program MolProbity (56). Data collection and refinement statistics for all structures are outlined in *SI Appendix*, Tables S1 and S2. All figures were generated with PyMOL (http://www.pymol.org).

Enzymatic Activity Assay. The neuraminidase activities of purified tNA, eNA, IBV NA, and 09N1 were measured using the fluorometric substrate 4-methylumbelliferyl *N*-acetyl-α-D-neuraminide (MUNANA or MUN) as described by Potier et al., with some modifications (57). Protein (10 μL) was mixed with 10 μL of buffer containing 33 mM 2-(*N*-morpholino)ethanesulfonic acid (MES) and 4 mM $CaCl_2$ (pH 6.0) in each well of a 96-well plate, after which the plate was incubated at 37 °C. The final concentrations were 20 nM for 09N1, 5 nM for tNA, 5 nM for eNA, and 5 nM for IBV NA. Serial twofold dilutions (final concentration range: 3.125 to 400 μM) of preheated MUNANA (30 μL) were then added to each well. The fluorescence intensity of released product was measured every minute over a period of 30 min at 37 °C on an Infinite M200 PRO multiplate reader (Tecan) at excitation and emission wavelengths of 355 and 460 nm, respectively. The reactions were all performed in triplicate and repeated three times. The K_m, which represents the affinity of the enzyme for the MUNANA substrate, and the maximum velocity of substrate conversion (V_{max}) were calculated using a nonlinear regression function with the Michaelis–Menten equation in GraphPad Prism.

NA Inhibition Assay. To evaluate the potency of NA inhibitors on tNA and eNA, NA inhibition assays using MUNANA were performed. At least six concentrations of each inhibitor at an appropriate range were used for each repeat. Inhibitor solutions were serially diluted 10-fold in fresh phosphate-buffered saline. Purified tNA protein (10 μL) and 10 μL inhibitor were coincubated for 30 min at room temperature. After incubation, 30 μL of 166 μM MUNANA in 33 mM MES buffer and 4 mM $CaCl_2$ (pH 6.0) was added to the solution to start the reaction. A positive control and a negative control were included in each experiment. Fluorescence was quantified every minute for 30 min at an excitation wavelength of 355 nm and an emission wavelength of 460 nm. At least three replicates were used for each condition, and the IC_{50} for each inhibitor was calculated using GraphPad Prism.

Phylogenetic Analysis. A phylogenetic tree was generated using the neighbor-joining cluster method of the ClustalW2 program on the EMBL-EBI server (58, 59) and visualized with iTOL (60). The following representative NA sequences were used to generate the phylogenetic tree of N1 to N11 and IBV NA subtypes: A/California/04/2009 (H1N1), A/RI/5+/1957 (H2N2), A/swine/Missouri/2124514/2006 (H2N3), A/mink/Sweden/E12665/84 (H10N4), A/duck/Alberta/60/1976 (H12N5), A/chicken/Nanchang/7010/2000 (H3N6), A/mallard/ALB/196/1996 (H10N7), A/duck/Ukraine/1/1963 (H3N8), A/tern/Australia/G70C/1975 (H11N9), A/bat/Guatemala/153/2009 (H17N10), A/bat/Peru/033/2010 (H18N11), B/Victoria/2/1987, and B/Yamagata/16/1988.

Data, Materials, and Software Availability. The structures determined in this study have been deposited in the Protein Data Bank with the following ID codes: 7FGB (apo-tNA) (61), 7FGC (tNA-zanamivir) (62), 7FGD (tNA-oseltamivir carboxylate) (63), 7FGE (tNA-peramivir) (64), 7XVR (apo-eNA) (65), 7XVV (eNA-zanamivir) (66), 7XVU (eNA-oseltamivir carboxylate) (67), and 7XVW (eNA-peramivir) (68).

All study data are included in the article and/or *SI Appendix*.

ACKNOWLEDGMENTS. We thank the staff of the BL02U1 and BL17U1 beamlines at the Shanghai Synchrotron Radiation Facility for data collection. This work was supported by the National Natural Science Foundation of China (Grant 31872745) and the National Key R&D Program of China (2020YFA0907104).

Author affiliations: [a]CAS Key Laboratory of Pathogen Microbiology and Immunology, Institute of Microbiology, Chinese Academy of Sciences (CAS), Beijing 100101, China; [b]University of Chinese Academy of Sciences, Beijing 100049, China; [c]Institute for Glycomics, Griffith University, Southport, QLD 4222, Australia; [d]College of Veterinary Medicine, China Agricultural University, Beijing 100193, China; [e]Shanxi Academy of Advanced Research and Innovation, Taiyuan 030032, China; [f]Laboratory of Protein Engineering and Vaccines, Tianjin Institute of Industrial Biotechnology, Chinese Academy of Sciences, Tianjin 300308, China; [g]School of Public Health (Shenzhen), Sun Yat-Sen University, Guangzhou 510080, China; [h]National Health Commission (NHC) Laboratory of Biosafety, National Institute for Viral Disease Control and Prevention, Chinese Center for Disease Control and Prevention (China CDC), Beijing 102206, China; and [i]Laboratory of Structural Biology, Tianjin Institute of Industrial Biotechnology, Chinese Academy of Sciences, Tianjin 300308, China

1. D. M. Knipe, P. M. Howley, *Fields Virology* (Wolters Kluwer/Lippincott Williams & Wilkins Health, Philadelphia, PA, 6th ed., 2013).
2. R. A. Lamb, "Influenza" in *Encyclopedia of Virology*, B. W. J. Mahy, M. H. V. Van Regenmortel, Eds. (Academic Press, Oxford, UK, 3rd ed., 2008), pp. 95–104.
3. C. J. Vavricka *et al.*, Special features of the 2009 pandemic swine-origin influenza A H1N1 hemagglutinin and neuraminidase. *Chin. Sci. Bull.* **56**, 1747–1752 (2011).
4. G. F. Gao, Influenza and the live poultry trade. *Science* **344**, 235 (2014).
5. S. Tong *et al.*, A distinct lineage of influenza A virus from bats. *Proc. Natl. Acad. Sci. U.S.A.* **109**, 4269–4274 (2012).
6. S. Tong *et al.*, New World bats harbor diverse influenza A viruses. *PLoS Pathog.* **9**, e1003657 (2013).
7. E. A. Moreira *et al.*, Synthetically derived bat influenza A-like viruses reveal a cell type- but not species-specific tropism. *Proc. Natl. Acad. Sci. U.S.A.* **113**, 12797–12802 (2016).
8. G. Zhong *et al.*, Mutations in the neuraminidase-like protein of bat influenza H18N11 virus enhance virus replication in mammalian cells, mice, and ferrets. *J. Virol.* **94**, e01416-19 (2020).
9. M. Shi *et al.*, The evolutionary history of vertebrate RNA viruses. *Nature* **556**, 197–202 (2018).
10. G. A. Arunkumar *et al.*, Functionality of the putative surface glycoproteins of the Wuhan spiny eel influenza virus. *Nat. Commun.* **12**, 6161 (2021).
11. R. Parry, M. Wille, O. M. H. Turnbull, J. L. Geoghegan, E. C. Holmes, Divergent influenza-like viruses of amphibians and fish support an ancient evolutionary association. *Viruses* **12**, 1042 (2020).
12. G. M. Air, W. G. Laver, The neuraminidase of influenza virus. *Proteins* **6**, 341–356 (1989).
13. C. Liu, M. C. Eichelberger, R. W. Compans, G. M. Air, Influenza type A virus neuraminidase does not play a role in viral entry, replication, assembly, or budding. *J. Virol.* **69**, 1099–1106 (1995).
14. P. Palese, K. Tobita, M. Ueda, R. W. Compans, Characterization of temperature sensitive influenza virus mutants defective in neuraminidase. *Virology* **61**, 397–410 (1974).
15. Y. Wu, Y. Wu, B. Tefsen, Y. Shi, G. F. Gao, Bat-derived influenza-like viruses H17N10 and H18N11. *Trends Microbiol.* **22**, 183–191 (2014).
16. R. J. Russell *et al.*, The structure of H5N1 avian influenza neuraminidase suggests new opportunities for drug design. *Nature* **443**, 45–49 (2006).
17. W. J. Liu *et al.*, Emerging HxNy influenza A viruses. *Cold Spring Harb. Perspect. Med.* **12**, a038406 (2022).
18. Q. Li *et al.*, Structural and functional characterization of neuraminidase-like molecule N10 derived from bat influenza A virus. *Proc. Natl. Acad. Sci. U.S.A.* **109**, 18897–18902 (2012).
19. X. Zhu *et al.*, Crystal structures of two subtype N10 neuraminidase-like proteins from bat influenza A viruses reveal a diverged putative active site. *Proc. Natl. Acad. Sci. U.S.A.* **109**, 18903–18908 (2012).
20. Y. Wu *et al.*, Resistance to mutant group 2 influenza virus neuraminidases of an oseltamivir-zanamivir hybrid inhibitor. *J. Virol.* **90**, 10693–10700 (2016).
21. Y. Wu *et al.*, Atypical group 1 neuraminidase pH1N1-N1 bound to a group 1 inhibitor. *Protein Cell* **6**, 771–773 (2015).
22. C. J. Vavricka *et al.*, Structural and functional analysis of laninamivir and its octanoate prodrug reveals group specific mechanisms for influenza NA inhibition. *PLoS Pathog.* **7**, e1002249 (2011).
23. C. U. Kim *et al.*, Influenza neuraminidase inhibitors possessing a novel hydrophobic interaction in the enzyme active site: Design, synthesis, and structural analysis of carbocyclic sialic acid analogues with potent anti-influenza activity. *J. Am. Chem. Soc.* **119**, 681–690 (1997).
24. M. von Itzstein *et al.*, Rational design of potent sialidase-based inhibitors of influenza virus replication. *Nature* **363**, 418–423 (1993).
25. P. M. Colman, J. N. Varghese, W. G. Laver, Structure of the catalytic and antigenic sites in influenza virus neuraminidase. *Nature* **303**, 41–44 (1983).
26. M. N. Janakiraman, C. L. White, W. G. Laver, G. M. Air, M. Luo, Structure of influenza virus neuraminidase B/Lee/40 complexed with sialic acid and a dehydro analog at 1.8-Å resolution: Implications for the catalytic mechanism. *Biochemistry* **33**, 8172–8179 (1994).
27. P. M. Colman, Influenza virus neuraminidase: Structure, antibodies, and inhibitors. *Protein Sci.* **3**, 1687–1696 (1994).
28. M. Richard *et al.*, Combinatorial effect of two framework mutations (E119V and I222L) in the neuraminidase active site of H3N2 influenza virus on resistance to oseltamivir. *Antimicrob. Agents Chemother.* **55**, 2942–2952 (2011).
29. A. J. Burnham *et al.*, Fitness costs for influenza B viruses carrying neuraminidase inhibitor-resistant substitutions: Underscoring the importance of E119A and H274Y. *Antimicrob. Agents Chemother.* **58**, 2718–2730 (2014).
30. R. Farrukee *et al.*, Influenza viruses with B/Yamagata- and B/Victoria-like neuraminidases are differentially affected by mutations that alter antiviral susceptibility. *J. Antimicrob. Chemother.* **70**, 2004–2012 (2015).
31. Y. H. Baek *et al.*, Profiling and characterization of influenza virus N1 strains potentially resistant to multiple neuraminidase inhibitors. *J. Virol.* **89**, 287–299 (2015).
32. C. Hanpaibool, M. Leelawiwat, K. Takahashi, T. Rungrotmongkol, Source of oseltamivir resistance due to single E119D and double E119D/H274Y mutations in pdm09H1N1 influenza neuraminidase. *J. Comput. Aided Mol. Des.* **34**, 27–37 (2020).
33. A. G. L'Huillier *et al.*, E119D neuraminidase mutation conferring pan-resistance to neuraminidase inhibitors in an A(H1N1)pdm09 isolate from a stem-cell transplant recipient. *J. Infect. Dis.* **212**, 1726–1734 (2015).
34. M. Okomo-Adhiambo *et al.*, Detection of E119V and E119I mutations in influenza A (H3N2) viruses isolated from an immunocompromised patient: Challenges in diagnosis of oseltamivir resistance. *Antimicrob. Agents Chemother.* **54**, 1834–1841 (2010).
35. Q. Li *et al.*, The 2009 pandemic H1N1 neuraminidase N1 lacks the 150-cavity in its active site. *Nat. Struct. Mol. Biol.* **17**, 1266–1268 (2010).
36. W. P. Burmeister, S. Cusack, R. W. Ruigrok, Calcium is needed for the thermostability of influenza B virus neuraminidase. *J. Gen. Virol.* **75**, 381–388 (1994).
37. N. J. Baker, S. S. Gandhi, Effect of Ca^{++} on the stability of influenza virus neuraminidase. *Arch. Virol.* **52**, 7–18 (1976).
38. X. Xu, X. Zhu, R. A. Dwek, J. Stevens, I. A. Wilson, Structural characterization of the 1918 influenza virus H1N1 neuraminidase. *J. Virol.* **82**, 10493–10501 (2008).
39. S. Li, J. Schulman, S. Itamura, P. Palese, Glycosylation of neuraminidase determines the neurovirulence of influenza A/WSN/33 virus. *J. Virol.* **67**, 6667–6673 (1993).
40. E. Bause, Structural requirements of N-glycosylation of proteins. Studies with proline peptides as conformational probes. *Biochem. J.* **209**, 331–336 (1983).
41. A. J. Oakley *et al.*, Structural and functional basis of resistance to neuraminidase inhibitors of influenza B viruses. *J. Med. Chem.* **53**, 6421–6431 (2010).
42. P. J. Collins *et al.*, Crystal structures of oseltamivir-resistant influenza virus neuraminidase mutants. *Nature* **453**, 1258–1261 (2008).
43. Y. Wu *et al.*, Characterization of two distinct neuraminidases from avian-origin human-infecting H7N9 influenza viruses. *Cell Res.* **23**, 1347–1355 (2013).
44. Y. Wu *et al.*, Induced opening of influenza virus neuraminidase N2 150-loop suggests an important role in inhibitor binding. *Sci. Rep.* **3**, 1551 (2013).
45. M. Wang *et al.*, Influenza A virus N5 neuraminidase has an extended 150-cavity. *J. Virol.* **85**, 8431–8435 (2011).
46. X. Sun *et al.*, Structure of influenza virus N7: The last piece of the neuraminidase "jigsaw" puzzle. *J. Virol.* **88**, 9197–9207 (2014).
47. Q. Li *et al.*, Functional and structural analysis of influenza virus neuraminidase N3 offers further insight into the mechanisms of oseltamivir resistance. *J. Virol.* **87**, 10016–10024 (2013).
48. W. Minor, M. Cymborowski, Z. Otwinowski, M. Chruszcz, HKL-3000: The integration of data reduction and structure solution–From diffraction images to an initial model in minutes. *Acta Crystallogr. D Biol. Crystallogr.* **62**, 859–866 (2006).
49. W. Kabsch, XDS. *Acta Crystallogr. D Biol. Crystallogr.* **66**, 125–132 (2010).
50. W. L. Bragg, E. R. Howells, X-ray diffraction by imidazole methaemoglobin. *Acta Crystallogr.* **7**, 409–411 (1954).
51. X. Zhu, X. Xu, I. A. Wilson, Structure determination of the 1918 H1N1 neuraminidase from a crystal with lattice-translocation defects. *Acta Crystallogr. D Biol. Crystallogr.* **64**, 843–850 (2008).
52. Z. Dauter, M. Jaskólski, Crystal pathologies in macromolecular crystallography. *Postepy Biochem.* **62**, 401–407 (2016).
53. A. Vagin, A. Teplyakov, MOLREP: An automated program for molecular replacement. *J. Appl. Crystallogr.* **30**, 1022–1025 (1997).
54. P. D. Adams *et al.*, PHENIX: A comprehensive Python-based system for macromolecular structure solution. *Acta Crystallogr. D Biol. Crystallogr.* **66**, 213–221 (2010).
55. P. Emsley, B. Lohkamp, W. G. Scott, K. Cowtan, Features and development of Coot. *Acta Crystallogr. D Biol. Crystallogr.* **66**, 486–501 (2010).
56. V. B. Chen *et al.*, MolProbity: All-atom structure validation for macromolecular crystallography. *Acta Crystallogr. D Biol. Crystallogr.* **66**, 12–21 (2010).
57. M. Potier, L. Mameli, M. Bélisle, L. Dallaire, S. B. Melançon, Fluorometric assay of neuraminidase with a sodium (4-methylumbelliferyl-alpha-D-*N*-acetylneuraminate) substrate. *Anal. Biochem.* **94**, 287–296 (1979).
58. F. Madeira *et al.*, The EMBL-EBI search and sequence analysis tools APIs in 2019. *Nucleic Acids Res.* **47**, W636–W641 (2019).
59. J. D. Thompson, T. J. Gibson, D. G. Higgins, Multiple sequence alignment using ClustalW and ClustalX. *Curr. Protoc. Bioinformatics*, chap. 2, unit 2.3 (2002).
60. I. Letunic, P. Bork, Interactive Tree of Life (iTOL) v4: Recent updates and new developments. *Nucleic Acids Res.* **47**, W256–W259 (2019).

61. Y. Chai, Y. Wu, F. Gao, A naturally-occurring neuraminidase-inhibitors-resistant NA from asiatic toad influenza B-like virus. Protein Data Bank. https://www.rcsb.org/pdb/explore/explore.do?structureId=7FGB. Deposited 26 July 2021.
62. Y. Chai, Y. Wu, F. Gao, A naturally-occurring neuraminidase-inhibitors-resistant NA from asiatic toad influenza B-like virus. Protein Data Bank. https://www.rcsb.org/pdb/explore/explore.do?structureId=7FGC. Deposited 26 July 2021.
63. Y. Chai, Y. Wu, F. Gao, A naturally-occurring neuraminidase-inhibitors-resistant NA from asiatic toad influenza B-like virus. Protein Data Bank. https://www.rcsb.org/pdb/explore/explore.do?structureId=7FGD. Deposited 26 July 2021.
64. Y. Chai, Y. Wu, F. Gao, A naturally-occurring neuraminidase-inhibitors-resistant NA from asiatic toad influenza B-like virus. Protein Data Bank. https://www.rcsb.org/pdb/explore/explore.do?structureId=7FGE. Deposited 26 July 2021.
65. Y. Chai, F. Gao, Structure of neuraminidase from influenza B-like viruses derived from spiny eel. Protein Data Bank. https://www.rcsb.org/pdb/explore/explore.do?structureId=7XVR. Deposited 24 May 2022.
66. Y. Chai, F. Gao, Structure of neuraminidase from influenza B-like viruses derived from spiny eel. Protein Data Bank. https://www.rcsb.org/pdb/explore/explore.do?structureId=7XVV. Deposited 24 May 2022.
67. Y. Chai, F. Gao, Structure of neuraminidase from influenza B-like viruses derived from spiny eel. Protein Data Bank. https://www.rcsb.org/pdb/explore/explore.do?structureId=7XVU. Deposited 24 May 2022.
68. Y. Chai, F. Gao, Structure of neuraminidase from influenza B-like viruses derived from spiny eel. Protein Data Bank. https://www.rcsb.org/pdb/explore/explore.do?structureId=7XVW. Deposited 25 May 2022.